Supporting Information

Disintegrating polymer multilayers to jump-start colloidal swimmers

Marina Fernández-Medina,[a] Xiaomin Qian,[a] Ondrej Hovorka,[b] and Brigitte Städler[a*]

[a]*Interdisciplinary Nanoscience Center (iNANO), Aarhus University, Gustav Wieds Vej 14, 8000 Aarhus (Denmark). bstadler@inano.au.dk.*

[b]*Faculty of Engineering and Physical Sciences, University of Southampton, SO16 7QF, Southampton, UK.*

Part I: Experimental aspects

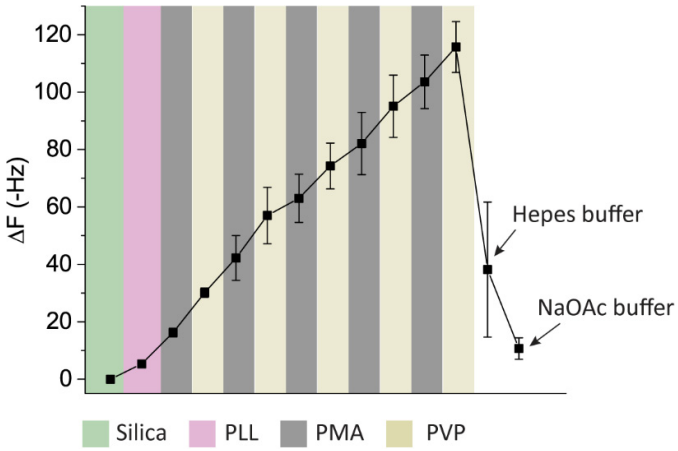

Figure S1. Film assembly: The change in frequency (Δf) of silica crystals upon deposition of PLL/$(PMA/PVP)_5$ using 10 kDa PVP and 15 kDa PMA during assembly in NaOAc buffer including the exposure of the assembled film to Hepes2 buffer and washing back to NaOAc buffer as monitored in QCM-D.

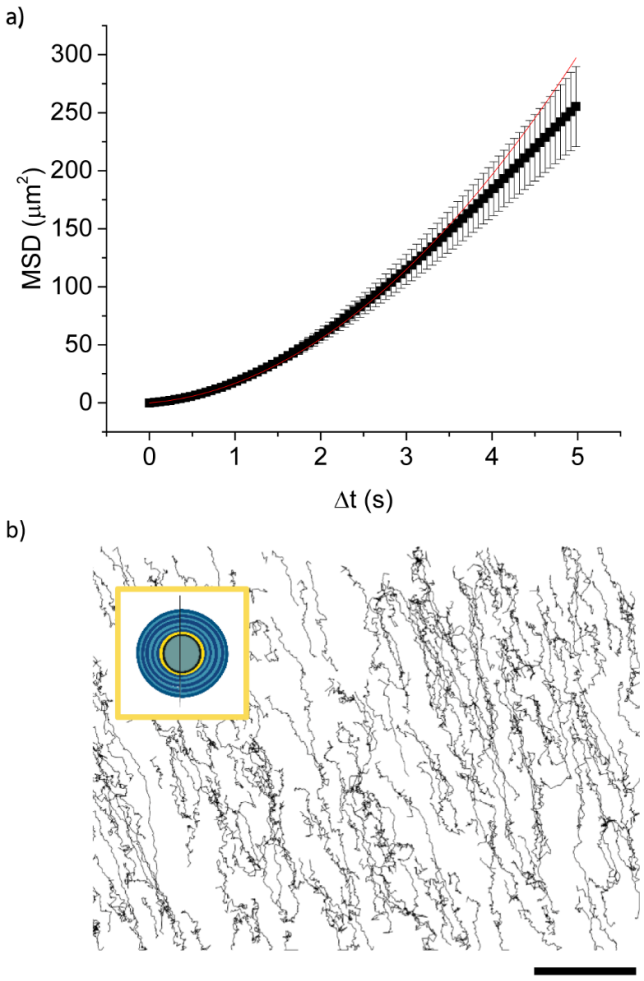

Figure S2. Region A: a) MSD analysis and b) representative trajectories of individual $S_{5\text{-}0.8}$ in Region A when 1 M NaOH was used to generate the pH gradient. Scale bar: 50 µm.

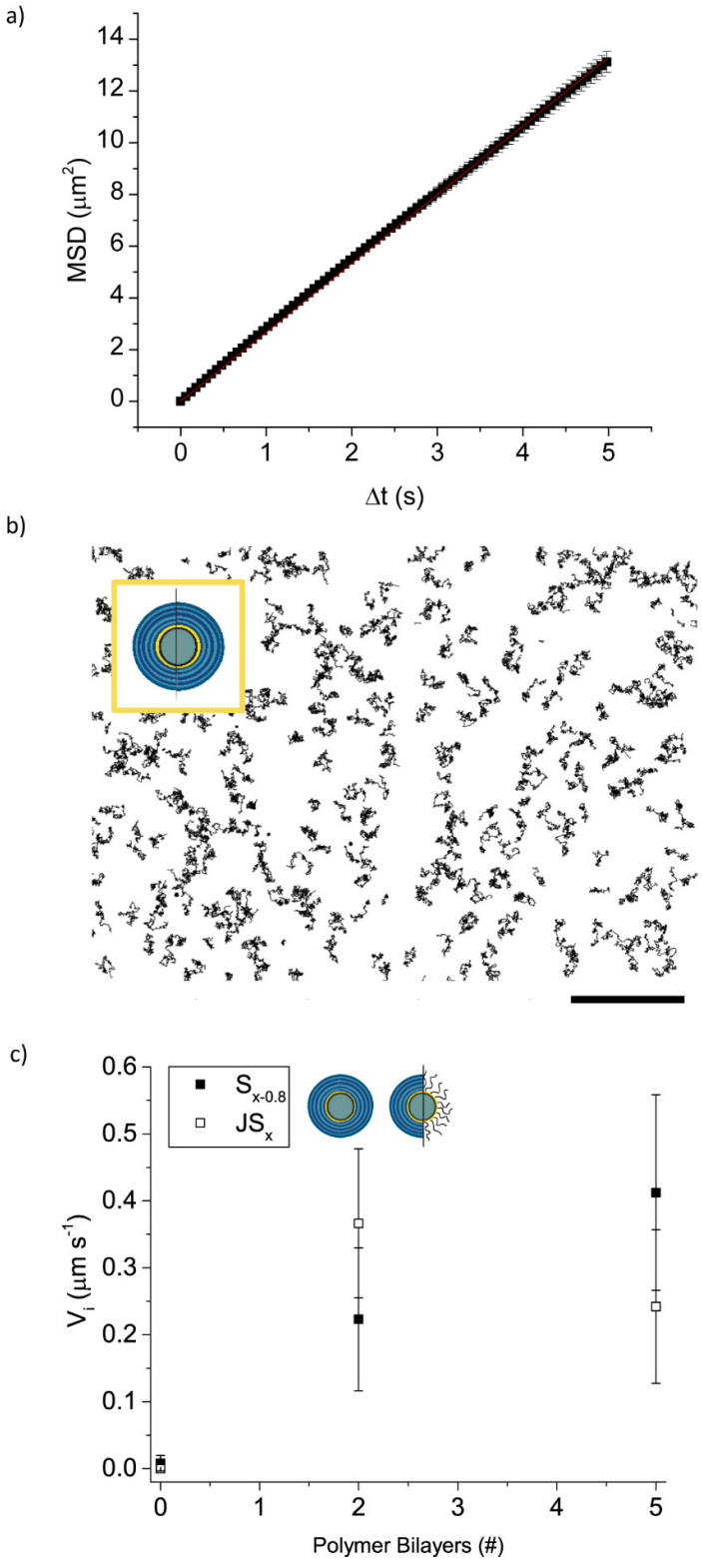

Figure S3. Region B: a) MSD analysis and b) representative trajectories of individual $S_{5\text{-}0.8}$ in Region B when 1 M NaOH was used to generate the pH gradient. Scale bar: 50 μm. c) Instantaneous velocity (v_i) of $S_{x\text{-}0.8}$ and $JS_{x\text{-}0.8}$.

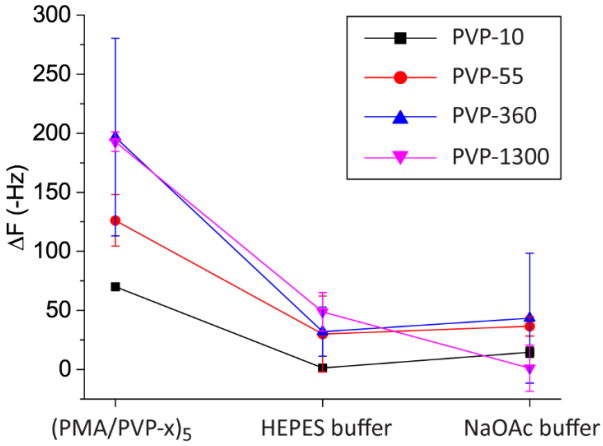

Figure S4. Total ∆f of silica crystal upon exposure to (PMA/PVP-x) using PVP with different MW during assembly in NaOAc buffer, followed by exposure to HEPES buffer and finally rinsing with NaOAc buffer.

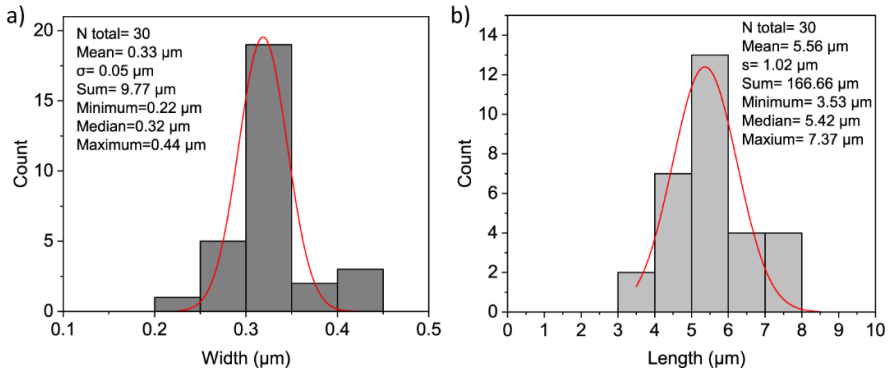

Figure S5. Rods size distribution – width (a) and length (b), aspect ratio (w:h) = 16.

Part II: Theoretical analysis

Here we present theoretical analysis of the swimming motion of particles observed in experiments. The aim is to develop simple models providing qualitative understanding of the data, rather than attempt quantitative analysis. The section split is as follows. 1) First we calculate one-dimensional pH profiles across the microfluidic channel as a function of position within the channel and time. 2) Then we calculate perturbation of this 'global' pH concentration profile due to the presence of a micro-particle in the channel. 3) Subsequently we define the notion of the phoretic velocity, which we use to evaluate phoretic velocities of fully polymer-coated and Janus swimmers. 4) We discuss the issue of the dependence of phoretic velocity on the mass of swimmers. 5) We also address the question of disordering the directional motion of swimmers by Brownian thermal fluctuations.

1 Distribution of pH across 'μ-Slides VI' microfluidic channel

Illustration of the experimental setup is shown in Fig. S6. The intake of NaOH occurs through the inlet at the left end of the channel, positioned in the coordinate system at $z' = 0$. We assume the reservoir supplies constant NaOH concentration $c(z' = 0, t) = c_0$ at all times t. The microfluidic channel (W $\times$ H $\times$ L = 3.8 mm $\times$ 0.4 mm $\times$ 17 mm) is much bigger than the particle size ($< \mu m$), and it can be assumed that particle causes only a perturbative modification to global concentration in the microfluidic channel. This allows us to first evaluate the concentration profile in the microfluidic channel without a particle present, and then study the perturbation due to the particle.

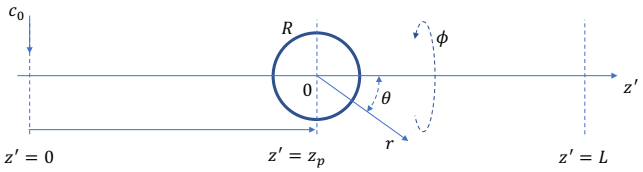

Figure S6: A sketch of the experimental setup showing two coordinate systems: the prime-d cartesian coordinate system associated with the microfluidic channel where the centre of the particle of radius R is located at coordinate $z' = z_p$, and the spherical coordinate system (r, θ, ϕ) associated with the particle and positioned at the particle centre.

Given that the length L of the channel dominates its width W and height H, the diffusion can be studied by assuming the variation of concentration only in z'-direction:

$$\frac{\partial c}{\partial t} = D \frac{\partial^2 c}{\partial z'^2} \tag{S1}$$

where D is the diffusion coefficient. The inlet boundary condition is $c(0, t) = c_0$ with c_0 being the concentration inflow as explained above. The right boundary condition $\partial c(L, t)/\partial z' = 0$ implies that the channel is closed-ended, i.e. with no concentration flux through the right boundary. The initial condition is $c(z', 0) = 0$ with the exception of $c(0, 0) = c_0$.

The solution to Eq. (S1) can be found by the Fourier method to be [1]:

$$\frac{c(z', t)}{c_0} = 1 - \frac{4}{\pi} \sum_{n=0}^{\infty} \frac{\sin\left(\frac{\pi}{2}(1+2n)\frac{z'}{L}\right)}{1+2n} \mathrm{e}^{-(1+2n)^2 t/\tau} \tag{S2}$$

where we denoted $\tau = \pi^2 D/(4L^2)$. Examples of solutions are shown in Fig. S7. Top figure shows the temporal evolution of the concentration profile suggesting that the propagating front (circles) slows down with increasing time. To define the concentration front we associate it with threshold concentration $c(z', t) = c_{tr}$. In practical terms, the threshold concentration c_{tr} corresponds to the resolution of the measurement, i.e. to the minimum concentration of the solvent that is detectable. We can then determine the time-dependence of the position x_{front} of the propagating front by numerically inverting Eq. (S2) and identifying the value of x_{front} for any given time t. The function $x_{\text{front}}(t)$ obtained in this way has been fitted to the experimental data shown in Fig. 1b in the main text, which allowed to determine

$^{a}\mathbf{c_{NaOH}}$ (M)	$^{b}\mathbf{D}$ ($\mathbf{cm^2s^{-1}}$)	$^{c}\mathbf{R^2}$
0.5	$5.16 \times 10^{-6} \pm 2.58 \times 10^{-6}$	0.953
1.0	$1.44 \times 10^{-5} \pm 0.72 \times 10^{-5}$	0.954
5.0	$6.49 \times 10^{-5} \pm 3.25 \times 10^{-5}$	0.926

Table S2: pH front propagation in a microfluidic channel. [a]3 μL NaOH, [b]Calculated diffusion coefficient, [c]Coefficient of determination.

the diffusion coefficient D as a fit parameter. The value of D was determined in this way for various choices of the threshold concentration c_{tr} and the range of the resulting values of D with acceptable fit quality ($R^2 > 0.9$) was used to identify the error bars in Table S2.

The bottom part of Fig. S7 shows the time-dependence of the concentration gradient. The concentration gradient is sharp at short times and flattens out as the time increases. Thus the pH gradient is expected to be more significant at the beginning of the microfluidic channel and decrease with the increasing distance, as highlighted in the figure by the two dashed lines corresponding to 4 mm (region A) and 9 mm (region B) markers for monitoring the particle velocities in the microfluidic channel (see the main text).

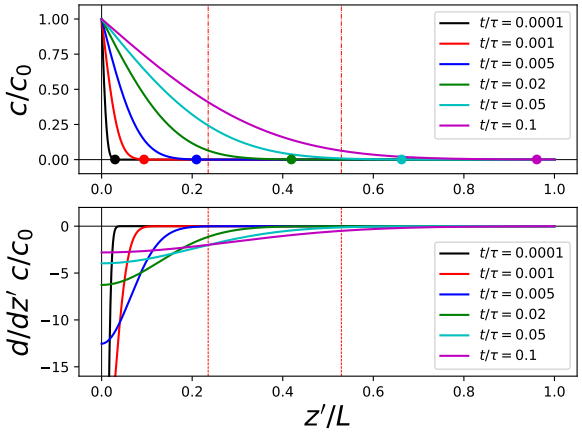

Figure S7: Concentration profiles (top) and concentration gradients (bottom) along the fluidic channel at different time instants. The dots in the top figure highlight the location of the propagating concentration front. According to Eq. (S2) the time constant $\tau = \pi^2 D/(4L^2)$ where D is the diffusion coefficient. The vertical dashed lines denote the 4 mm and 9 mm locations along the microfluidic channel.

2 Concentration profile induced by a particle

In calculations below, we will take advantage of small dimensions of particles used in experiments ($< \mu$m) in comparison to the size of the microfluidic channel (mm). **Assumption 1:** Then it is expected that the concentration profile established in the previous section becomes modified by the particle only in its proximity and that it can be locally linearised. **Assumption 2:** We will also assume that the motion of a particle occurs at timescales shorter (fast particles) than the timescale of the propagating front (slow front). This assumption is valid only approximately as both the particle and front propagation velocities are in the range from 1-10 μms^{-1} (compare Fig. 1b and Fig. 2a in the main text). Nevertheless, these assumptions will be shown below to lead to a reasonable interpretation of the experimental data.

2.1 Linearisation of the concentration gradient along the particle

Given the small size of particles (assumption 1 above) it is plausible to approximate the concentration profile given by Eq. (S2) at any particle position z_p by a linear function following from the Taylor

expansion around z_p:

$$c(z') = c(z_p) + \frac{\partial c(z_p)}{\partial z'}(z' - z_p) + \dots \tag{S3}$$

This equation can be rewritten in the local coordinate system of the particle (Fig. S6) as:

$$c(z + z_p) = c(z_p) + \frac{\partial c(z_p)}{\partial z} z + \dots \tag{S4}$$

where $z = z' - z_p$ is the z coordinate in the local coordinate system of the particle. Recalling that in spherical coordinates $z = r\cos\theta$, we can rewrite the above equation as:

$$\begin{aligned} c(r, \theta) &= c(z_p) + \frac{\partial c(z_p)}{\partial z} r\cos\theta \\ &= c(z_p) + \lambda r \cos\theta \end{aligned} \tag{S5}$$

where we introduced the symbol λ as short notation for the gradient. Eq. (S5) will serve as a far-field boundary condition for the solution of the particle proximity concentration profile, discussed next.

2.2 Axially symmetric concentration profile around the particle

Assuming the temporal variation of the global concentration in the microfluidic channel is not significant at the characteristic timescales of the particle motion (see Assumption 2 above), the concentration in the proximity of a particle can be studied by solving the diffusion equation with neglected time derivative:

$$D\nabla^2 c = 0 \tag{S6}$$

This equation is complemented by the far-field boundary condition given by Eq. (S5), and the following 'surface' boundary condition applied on the particle surface [2]:

$$-D\hat{n} \cdot \nabla c(\vec{r}_s) = \alpha(\vec{r}_s) \tag{S7}$$

where the unit vector $\hat{n}$ represents a normal to the particle surface and α is the surface activity induced by chemical processes at the position $\vec{r}$ on the particle surface. Surface activity $\alpha > 0$ ($\alpha < 0$) represents generation (consumption) of solute by chemical reaction.

Assuming azimuthal symmetry, general solutions of Eq. (S6) can be expressed as:

$$c(r, \theta) = \sum_{l=0}^{\infty} (A_l r^l + B_l r^{-(l+1)}) P_l(\cos\theta) \tag{S8}$$

where P_l represents Legendre polynomials of the order $l \geq 0$, and A_l and B_l are coefficients to be determined from boundary conditions Eq. (S5) and (S7). Examples of the first few Legendre polynomials are:

$$P_0(x) = 1 \qquad P_1(x) = x \qquad P_2(x) = \frac{1}{2}(3x^2 - 1) \tag{S9}$$

The long-distance limit $r \to \infty$ of Eq. (S8) needs to recover the far-field concentration given by Eq. (S5), which immediately implies:

$$\begin{aligned} A_0 &= c(z_p) \\ A_1 &= \lambda \\ A_l &= 0 \quad \text{for} \quad l > 1 \end{aligned} \tag{S10}$$

since $P_1(\cos\theta) = \cos\theta$.

To apply the surface boundary condition Eq. (S7), we first expand the surface activity $\alpha(\theta)$ in the series of Legendre polynomials:

$$\alpha(\theta) = \sum_{l=0}^{\infty} \alpha_l P_l(\cos\theta) \tag{S11}$$

Inserting Eqs. (S8) and (S11) into (S7) and arranging allows to express the B_l as:

$$B_l = \frac{\alpha_l + D\lambda\delta_{1l}}{D(l+1)} R^{l+2} \tag{S12}$$

where $\delta_{1l} = 1$ if $l = 1$ and $\delta_{1l} = 0$ for $l \neq 0$.

Entering the coefficients A_l and B_l in Eq. (S8) and arranging, the solution for concentration reads:

$$c(r,\theta) = c(z_p) + \lambda r \cos\theta \left(1 + \frac{1}{2}\frac{R^3}{r^3}\right) + \frac{R}{D}\sum_{l=0}^{\infty} \frac{\alpha_l}{l+1}\left(\frac{R}{r}\right)^{l+1} P_l(\cos\theta) \tag{S13}$$

It can be checked that the long-distance limit $r \to \infty$ of Eq. (S13) recovers the solution given by Eq. (S5). On the particle surface when $r = R$, the solution recovers the boundary condition given by Eq. (S7). In the absence of the pH gradient $\lambda = 0$, and Eq. (S13) loses the second term and reduces to the expression found earlier [2].

Eq. (S13) suggests that there is a concentration variation due to the presence of a particle even if the surface activity $\alpha = 0$, as is expected. As will be shown below, this variation gives rise to a non-zero 'phoretic' velocity of uncoated particles and adds a velocity contribution in case of the fully polymer-coated and Janus particles, which is consistent with our experimental observations in Figures 2-4 in the main part of the article. This is the key difference between this and the earlier theoretical work [2].

3 Phoretic velocity of a particle

The phoretic velocity of a particle projected onto the $\hat{z}$ direction can be defined by the following surface integral [2, 3, 4]:

$$v_{ph} = \vec{v}\cdot\hat{z} = -\frac{1}{4\pi R^2}\oint_S dS\,\mu(\vec{r}_S)\hat{z}\cdot(\mathbb{I} - \hat{n}\hat{n})\cdot\nabla c(\vec{r}_S) \tag{S14}$$

where μ is the diffusioosmotic coefficient and $\mathbb{I}$ is the unit matrix. Assuming axial symmetry, this expression reduces to simpler form:

$$v_{ph} = \frac{1}{2R}\int_0^{\pi} d\theta \sin^2\theta\mu(\theta)\frac{\partial c(R,\theta)}{\partial\theta} \tag{S15}$$

Expressing $\mu(\theta)$ in the series of Legendre polynomials:

$$\mu(\theta) = \sum_{l=0}^{\infty}\mu_l P_l(\cos\theta) \tag{S16}$$

and inserting Eq. (S13) in Eq. (S15) gives after arranging the following expression for the phoretic velocity of a particle:

$$v_{ph} = -\lambda\mu_0 + \frac{1}{5}\lambda\mu_2 - \frac{1}{D}\sum_{l=0}^{\infty}\frac{l+1}{2l+3}\alpha_{l+1}\left(\frac{\mu_l}{2l+1} - \frac{\mu_{l+2}}{2l+5}\right) \tag{S17}$$

This expression allows to evaluate the phoretic velocity of a particle if the surface functions μ and α are known. Below we discuss three specific cases, of a particle without surface activity, and of fully polymer-coated and Janus particles (Figure S8).

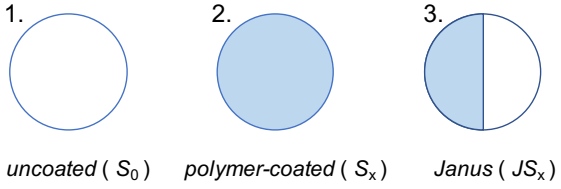

Figure S8: Particle types considered in the study: uncoated particles S_0, fully polymer-coated particles S_x, and half-coated Janus particles JS_x.

3.1 Phoretic velocity of non-coated particle (S_0)

First we consider the case of a particle without the surface activity, which implies all coefficients $\alpha_l = 0$ in Eq. (S17). Then, assuming the diffusioosmotic coefficient is constant over the particle surface and equal to μ_0, we set $\mu_2 = 0$ (note that $\mu_2 \neq 0$ would mean $\cos\theta$-like variation, see Eq. (S16)). With these considerations Eq. (S17) reduces to:

$$v_{ph} = -\lambda\mu_0 = -\frac{\partial c(z_p)}{\partial z}\mu_0 \tag{S18}$$

The global concentration gradient in the microfluidic channel is always negative, and therefore the swimming occurs in the positive z-direction. Thus a particle (even uncoated) will move in the positive direction towards the reduced concentration gradient.

3.2 Phoretic velocity of a fully polymer-coated particle ($S_{x-0.8}$)

Next we consider a fully polymer-coated particle. Again, we take a constant diffusioosmotic coefficient equal to μ_0, but now assume that the surface activity is a function of the global concentration gradient in the microfluidic channel:

$$\alpha(\theta) = \mathcal{F}(c(z')) \tag{S19}$$

where the symbol $\mathcal{F}$ denotes some unknown functional form of the concentration dependence of α. The functional form of $\mathcal{F}$ depends on the details of the kinetics of chemical reactions occurring at the particle surface. Due to the limited reaction surface, behaviour displaying saturating trend leading to a non-linear functional form of $\mathcal{F}$ is expected.

To simplify mathematical calculations, we will assume linear relation between the surface activity and the NaOH solute concentration (pH level):

$$\mathcal{F}(c(z')) \approx \alpha_f c(z') = \alpha_f \cdot (c(z_p) + \lambda R\cos\theta) \tag{S20}$$

where α_f is a proportionality constant and the last equality follows from Eq. (S5). The assumption of linearity is justifiable only for small concentrations of the NaOH solute. The factor α_f is expected to depend on the thickness of the polymer layer and the details of the kinetics of the chemical reactions occurring at the particle surface.

Setting in Eq. (S17) the coefficient $\alpha_0 = \alpha_f c(z_p)$ and $\alpha_1 = \alpha_f \lambda R$, and $\alpha_l = 0$ for all $l > 1$ allows to evaluate the phoretic velocity immediately as:

$$\begin{aligned} v_{ph} &= -\lambda\mu_0 - \frac{1}{3}\frac{\alpha_f \lambda R \mu_0}{D} \\ &= -\frac{\partial c(z_p)}{\partial z}\mu_0\left(1 + \frac{\alpha_f R}{3D}\right) \end{aligned} \tag{S21}$$

Because the concentration gradient is negative, swimming occurs in the positive z-direction. Moreover, the phoretic velocity is enhanced relative to the previous case of the uncoated particle because the phoretic activity triggered by polymer disintegration contributes to the local concentration of the solute ($\alpha_f > 0$).

3.3 Phoretic velocity of a Janus particle (JS_x)

For a Janus swimmer we assume similar conditions, i.e. constant phoretic mobility equal to μ_0, but the surface activity expected only on the left part of the particle covered by the polymer coating (Fig. S8):

$$\alpha(\theta) = \begin{cases} 0 & \text{if } 0 < \theta < \pi/2 \\ \alpha_f[c(z_p) + \lambda R\cos\theta] & \text{if } \pi < \theta < \pi/2 \end{cases} \tag{S22}$$

Then it can be shown by expanding $\alpha(\theta)$ into the series of Legendre polynomials that the only relevant expansion coefficient is $\alpha_1 = -3/4\alpha_f c(z_p) + 1/2\alpha_f \lambda R$, and using this in Eq. (S17) gives the phoretic

velocity as:

$$\begin{aligned} v_{ph} &= -\lambda\mu_0 - \frac{1}{6}\frac{\alpha_f \lambda R \mu_0}{D} + \frac{1}{4D}\alpha_f c(z_p)\mu_0 \\ &= -\frac{\partial c(z_p)}{\partial z}\mu_0\left(1 + \frac{\alpha_f R}{6D}\right) + \frac{1}{4D}\alpha_f c(z_p)\mu_0 \\ &\approx -\frac{\partial c(z_p)}{\partial z}\mu_0\left(1 + \frac{\alpha_f R}{6D}\right) \end{aligned} \tag{S23}$$

where we neglected the last term assuming it is small, which is reasonable in the high concentration gradient region. Comparing this expression with the phoretic velocity of the fully polymer-coated swimmer given by Eq. (S21) we see that Janus swimmers may be expected to be slower. The diffusioosmotic coefficient μ_0 should also be expected to be different for Janus particles than for fully coated particles, as it now needs to be interpreted as an effective value averaged over both the active and inactive halfs of the Janus particle.

The ratio between the phoretic velocities of the fully polymer-coated and Janus particles obtained by dividing Eqs. (S21) and (S23) is:

$$\frac{v_{ph}^{\mathrm{Sx}}}{v_{ph}^{\mathrm{JSx}}} = \frac{\mu_0^{\mathrm{Sx}}}{\mu_0^{\mathrm{JSx}}}\frac{1 + \alpha_f R/(3D)}{1 + \alpha_f R/(6D)} \approx 2\frac{\mu_0^{\mathrm{Sx}}}{\mu_0^{\mathrm{JSx}}} \tag{S24}$$

where the superscripts Sx and JSx refer to the fully coated and Janus particles, respectively, and the approximation on the right-hand side holds if $\alpha_f R/(6D) >> 1$. Considering our measurements in Figure 2a-i in the main text, we find that the ratio between the velocities of the fully polymer-coated and Janus swimmers is indeed not far from 2, and deviations can be attributed to the expected differences in the diffusiophoretic coefficients of the two types of swimmers.

4 Effect of particle mass

Velocity v_{ph} obtained in Eqs. (S18), (S21), and (S23), appears to be mass independent. This is because the theoretical evaluation of velocity is based only on the surface-fluid interactions and the inertial effects are not included. To estimate the effect of mass we consider the following very simple scenario. Initially, as soon as the particle is exposed to the transient concentration gradient, chemical activity will trigger accelerated particle motion. Because the particle moves in a fluid of viscosity η, it will experience Stokes viscous drag in the opposite direction. To describe this scenario, we can write simple Newton equation:

$$m\frac{dv}{dt} = -6\pi\eta R v + F \tag{S25}$$

where m is the mass of the particle, v is the actual velocity of the particle accelerating in the z-direction, and F is the phoretic force. The force F can be related to the phoretic velocity obtained in the previous section as $v_{ph} = \kappa F$, where κ is the mobility of the particle. Although we are unable to estimate κ at this time, we expect it to depend on the environment the particle is embedded in, and its interactions with the particle surface. For the purpose of the present study it will be sufficient to assume that κ is the same for particles of different size, if the material properties of particles and their environment are the same.

Assuming F is constant (because v_{ph} and κ are constant for a given particle), and in view of the assumption 2 in Section 2 above, integrating Eq. (S25) gives for the velocity the following expression:

$$v = \frac{F}{6\pi\eta R}\left(1 - \exp\left(-\frac{6\pi\eta R}{m}t\right)\right) \tag{S26}$$

Taking the long time limit $t \to \infty$ of this expression gives the steady state velocity as:

$$v_{\mathrm{steady}} = \frac{F}{6\pi\eta R} = \frac{v_{ph}}{6\pi\eta\kappa R} = \Omega\frac{v_{ph}}{m^{1/3}} \tag{S27}$$

where the constant $\Omega = (4\pi\rho)^{1/3}/(3^{1/3}6\pi\eta\kappa)$, and we used the relation $v_{ph} = \kappa F$ and the fact that $m = \rho V$ with the volume of a spherical particle $V = 4/3\pi R^3$ and ρ being the particle material density.

Thus in viscous environments we expect $m^{1/3}$ reduction of the steady state velocity v_{steady} of particles with increasing mass m, which is indeed what we find experimentally in Figure 4b in the main text.

Note that this conclusion requires assuming η, κ, and ρ to be the same for all particles with different mass, which is reasonable given that the particles in figure 4b are of the same material and the properties of the environment are the same for all the studied particle cases.

5 Brownian motion

Thermal fluctuations will disorder the particle motion away from the directed motion. It can be shown that this disordering effect occurs over the mean squared distance [5]:

$$\Delta z^2 = 4D\Delta t + \frac{v_{\text{steady}}^2 \tau_R^2}{2}\left(\frac{2\Delta t}{\tau_R} + \mathrm{e}^{-2\Delta t/\tau_R} - 1\right) \tag{S28}$$

where v_{ph} is the velocity evaluated in Eq. (S27) and $\tau_R = 8\pi\eta R^3/k_B T$ is the characteristic timescale of the rotational diffusion. The long time limit of this equation reduces to:

$$\Delta z^2 = 4D\Delta t + v_{\text{steady}}^2 \tau_R \Delta t \tag{S29}$$

which is the expression referred to in the main text (Movie Tracking, p. 3) and used for interpreting the velocities in experiments. When the velocity v_{steady} is significant, such as in the early left part of the microfluidic channel when the concentration gradient of the solute is high, the first term in Eq. (S29) can be neglected and the motion is directional. This is consistent with the observations in Figure 2a-i in the main text. On the other hand, as the concentration gradient reduces in the later locations of the microfluidic channel, the velocity reduces as well, and so does the second term in Eq. (S29). Then the motion of the swimmers if fully diffusive. This is indeed observed in Figure 2a-ii in the main part of the text.

References

[1] K. F. Riley, M. P. Hobson, and S. J. Bence, *Mathematical methods for physics and engineering*, AAPT (1999).

[2] R. Golestanian, T. B. Liverpool, A. Ajdari, New Journal of Physics **9**, 126 (2007).

[3] J. Anderson, Annual Review of Fluid Mechanics **21**, 61 (1989).

[4] S. Michelin, E. Lauga, Scientific Reports **7**, 42264 (2017).

[5] J. R. Howse, R. A. L. Jones, A. J. Ryan, T. Gough, R. Vafabakhsh, R. Golestanian, Physical Review Letters **99**, 048102 (2007).